Science & Technology Development Journal, 24(3):2011-2018

Open Access Full Text Article

Research Article

Effects of the hybrid plasmonic Ag/$SrTiO_3$ nanocubes for efficient photo-catalytic of H_2 generation and RhB decomposition

Ton Nu Quynh Trang[1,2], Le Lam Anh Phi[1,2], Le Thi Ngoc Tu[3], Vu Thi Hanh Thu[1,2,*]

[1]*Faculty of Physics and Physics Engineering, University of Science, Ho Chi Minh City 700000, Vietnam*

[2]*Vietnam National University, Ho Chi Minh City 700000, Vietnam*

[3]*Dong Thap University, Cao Lanh City, Dong Thap Province 870000, Vietnam*

Correspondence

Vu Thi Hanh Thu, Faculty of Physics and Physics Engineering, University of Science, Ho Chi Minh City 700000, Vietnam

Vietnam National University, Ho Chi Minh City 700000, Vietnam

Email: vththu@hcmus.edu.vn

History

- Received: 2021-05-24
- Accepted: 2021-07-25
- Published: 2021-08-02

DOI : 10.32508/stdj.v24i3.2568

ABSTRACT

Introduction: Designing a novel photocatalyst toward the photo-catalytic degradation of dye molecules and hydrogen evolution reaction (HER) based on semiconductors has been drawn enormous attention as a potential strategy in the clean energy field and environmental treatment. Herein, a $SrTiO_3$ (STO) nanocubes decorated with co-catalysts Ag nanoparticles (NPs) for H_2 generation and organic dye Rhodamine B (RhB) photodegradation activity under UV and visible light irradiation was fabricated. **Method**: The crystallinity, morphology, and chemical components of the photocatalyst were characterized through X-ray powder diffraction (XRD), scanning electron microscopy (SEM) equipped with energy-dispersive X-ray spectroscopy (EDX), respectively. The optical properties were evaluated through the UV-Visible absorbance spectra. **Results**: As a result, the photo-catalytic performance of the obtained Ag/STO hybrid photocatalyst was higher than that of the pristine STO nanocubes due to i) the efficient charge separation and transfer of photogenerated electron-holes pairs; ii) the improvement of the light-harvesting efficacy in the visible light. The high photo-catalytic RhB decomposition of the achieved Ag/STO hybrid photo-catalytic was obtained compared to the pure SrTiO3 nanocubes under UV and visible light exposure. The H_2 generation of Ag/STO photocatalyst was 2- and 12-time higher than that of the pure STO nanocubes under UV and visible light illumination, respectively. **Conclusion**: This study gives a general strategy for photocatalyst design towards water splitting for photo-catalytic H_2 evolution and environmental deterioration.

Key words: SrTiO3, hybrid structures, photo-catalytic activity, Ag nanoparticles

INTRODUCTION

Achieving the global energy demand and environmental sustainability is an ideal approach for the growth of clean energy to address the global energy crisis and environmental concerns[1,2]. Therefore, many technologies have been proposed for a cleaner environment and fossil energy alternatives. Among these, the production of hydrogen from solar-driven water-splitting reactions employing semiconductor nanomaterials as photocatalyst has a huge potential for replacement from conventional fossil fuels to renewable energy sources since the work of Honda and Fujishima was reported in the 1970s[3]. In principle, the activity of the water-splitting process based on semiconductor nanomaterials is highly influenced by the appropriate alignment of the valence band (VB) and the conduction band (CB) edges, thigh mobility of the charge carriers, the stability in an aqueous environment, and harvesting solar light capability[4–6]. In this sense, the perovskite oxide family, with its ABO_3 stoichiometry, especially $SrTiO_3$ (STO), were extensively postulated as a potential photocatalyst to produce photo-catalytic H_2 from aqueous solutions due to the structural and compositional flexibility allowing A- and B-site replacement in the crystal structure[7,8]. Moreover, CB of STO has more negative potential than the H^+/H_2 potential (0 V vs. NHE, at pH = 0), therefore supplies favorable redox potential for photo-catalytic water splitting into H_2 gas, leading to enhanced photo-catalytic efficiencies. From that time, many efforts based on perovskite materials have been explored[9–12]. However, the energy conversion efficiency of photo-catalytic water splitting into H_2 is still low due to i) STO can only be activated by UV light because of its wide forbidden energy of 3.2 eV; ii) the recombination rate of photogenerated electron-hole couples is rapid. Several effective strategies to address these intrinsic drawbacks of STO have been proposed, such as the use of co-catalysts[13,14], doping metal into the bandgap[15,16], incorporating with other oxide metal[17,18]. Among these approaches, the use of co-catalysts has been considered as one of the most promising approaches for enhanced photo-catalytic H_2 generation. Recently, plasmonic nanomaterials have attached considerable concerns in the field of photo-catalytic activity related to the localized surface

Cite this article : Trang T N Q, Phi L L A, Tu L T N, Thu V T H. **Effects of the hybrid plasmonic Ag/$SrTiO_3$ nanocubes for efficient photo-catalytic of H_2 generation and RhB decomposition**. *Sci. Tech. Dev. J.;* 24(3):2011-2018.

plasmon resonance (LSPR) and the formation of the Schottky barrier at the interface between metal and semiconductor. In view of these characteristics, noble metals using as co-catalyst are expected to advantage photo-catalytic H_2 evolution as well. The vital role of the co-catalyst is to enable visible light absorption and prolong the lifetime of photoinduced charge carriers. Some previous studies reported that coupling plasmonic nanostructures such as Ag, Au for water splitting could achieve higher photo-catalytic rates. For example, Yan et al. reported that loading Au onto $CaTiO_3$ composites exhibit highly enhanced photocatalytic performance compared to pristine $CaTiO_3$ due to an effective separation and transportation of photoinduced electron/hole pairs in $CaTiO_3$ and the LSPR effect of Au[19]. Guo et al. showcased that Al incorporated with $BaTiO_3$ exhibited excellent photocatalytic water splitting and pollutant degradation based on the piezoelectric polarization of $BaTiO_3$ and plasmonic activities of Al nanoparticles[20]. Another work reported that $Au_x/BaTiO_3$ plasmonic photocatalysts endowed a large light absorption from 300 to 600 nm. The results exhibited a high photo-catalytic performance for MO decomposition under solar light illumination of $Au_x/BaTiO_3$ nanocubes[21]. Based on these phenomena, herein, we demonstrate that loading Ag nanoparticles on well-defined STO nanocubes (Ag/STO) can effectively improve the photo-catalytic H_2 evolution from water splitting under visible light-responsive photocatalyst. The obtained photocatalyst are prepared via a facile and cost-effective route, in which STO nanocubes are fabricated by hydrothermal approach and loaded Ag nanoparticles through chemical reduction method under UV light irradiation. The morphological and crystal characteristics, optical properties, compositions, and photo-catalytic activity of the achieved Ag/STO heterojunctions were evaluated in detail. The results reveal that the heterostructured photocatalyst shows a greatly enhanced photo-catalytic efficiency on H_2 generation and the degradation of organic dyes under the illumination of UV and visible light compared with bare STO due to an efficient separation and transfer of photogenerated charge carriers and an improvement in the optical absorption ability.

MATERIALS - METHODS

Materials

Titanium dioxide (TiO_2, Merck, 99%), strontium nitrate ($Sr(NO_3)_2$, Sigma-Aldrich <99%), hydrochloric acid fuming (HCl, Merck, <37%), sodium hydroxide (NaOH, Merck, 99%), methanol (Merck, CH_3OH, <99.9%), rhodamine B (RhB, $C_{28}H_{31}ClN_2O_3$, >98% purity, Merck) and silver nitrate ($AgNO_3$, Merck, >=99). The chemical reagents were employed without any further purification. Double distilled water was used overall in the experiment.

Synthesis of $SrTiO_3$ (STO) nanocubes

STO nanocubes have been fabricated by hydrothermal approach as described in our study[22]. The schematic for the fabrication of STO is presented in Schematic 1. In a typical synthesis, 20 mL of a 0.5 M $TiCl_4$ aqueous solution was dissolved in 60 mL of DI and vigorously stirred for 30 min. After that, a suitable amount of $Sr(NO_3)_2$ was put into the above solution and continually stirred. Then, 10 ml of 2M KOH solution was dropped into the above reaction mixture and stirred for 30 minutes. The achieved suspension was transferred in a closed Teflon-lined autoclave at 210 °C for 4 h. The precipitates were collected using the centrifugation process and washed several times with double-distilled water. In the end, the sample was dried at 100 °C to obtain the final specimen.

Synthesis of Ag loaded onto the STO photocatalyst (Ag/STO)

Ag/STO photocatalyst was achieved by the photoreduction method. In detail, STO (30mg) was dispersed into the $AgNO_3$ aqueous solution under stirring. The reaction mixture was irradiated under a 300 W Xe lamp at room temperature for 1 hour. After the irradiation process, the grey products were gathered using the centrifugation process, washed with double water several times, and dried at 60 °C overnight.

Materials characterization

Powder X-ray diffraction (XRD) patterns of the as-obtained photocatalyst were acquired using X-ray diffractometry (Bruker D8 ADVANCE) equipped with Cu Kα radiation (α = 1.54056 Å). Morphological characterization of the samples was evaluated using a transmission electron microscope (TEM), field-emission scanning electron microscopy (FE-SEM) equipped with energy disperse X-ray spectrometer (EDX). The optical absorption of the photocatalyst was assessed by UV−visible diffuse reflectance spectroscopy (V-650, JASCO) at room temperature. Raman scattering spectra of the as-prepared was recorded by a Horiba XploRA PLUS Raman System at an excitation wavelength of 532 nm.

The photo-catalytic activity for H_2 evolution reaction (HER)

The photo-catalytic HER activity of samples was carried out in a Pyrex cell closed gas-circulation system. A Xe lamp (Cermax, 300 W) was utilized as the light source. In a typical process, 10 mg of the photocatalyst was dispersed in 40 mL of the aqueous solution containing 25 vol % methanol as the sacrificial agent and the reaction mixture was sonicated for 30 min to achieve a well-dispersed particle suspension. Before the light irradiation, the suspension was sealed and vacuumed for 30 min to ensure an inert environment. Then, the suspension was exposed under a 300 W xenon lamp equipped with a band-cutoff filter (420 nm). The H_2 evolution was monitored by gas chromatography with a thermal conductivity detector (TCD).

Photo-catalytic decomposition of the RhB molecules Dye

The photo-catalytic activity of the as-achieved photocatalyst was controlled under UV light (365 nm) and visible light irradiation for 150 min (Xe lamp, 300 W). Prior to light illumination, the mixture of aqueous RhB solution and the photocatalyst was placed in a dark. The remaining RhB concentration was investigated through a UV−vis spectrophotometer at the wavelength of 554 nm. The % decomposition of RhB dye was evaluated using the equation:

RhB decomposition (%) = $[(C_0\text{-}C_t)/C_0]$ ´100

Where, C_o and C_t are the RhB concentration at the initial time and after irradiation for time "t", respectively.

RESULTS

The detailed morphological characteristics of the as-prepared STO and Ag/STO nanocubes were investigated via SEM and TEM analyses. As shown in Figure 1(a), the pristine STO exhibits 3D nanostructures with an average particle size of ca.300 nm and an almost perfect cubic structure with six isotropic {100} facets. As mirrored in Figure 1(b), structures of Ag/STO are analogous to those of STO. Moreover, after photo-deposition of the Ag NPs on STO, a large number of Ag nanoparticles with the particle size of ca.30 nm was assembled on the whole STO surface, as marked by the yellow arrows (Figure 1(b)). As shown in Figure 1(b), the Ag atoms were not easily discovered as separate particles on the surface of STO, implying the Ag atoms were homogeneously deposited on the STO. The TEM image in Figure 1(c) reveals the nanocubes of Ag/STO with almost the same size as STO, indicating that Ag assembly did not change the morphological features of STO structures, which is consistent with SEM images. The EDX mapping images show the presence of Sr, Ti, O, and Ag elements of Ag/STO photocatalyst as presented in Figure 1(d-h), suggesting that Ag nanoparticles were deposited successfully on STO nanocubes via photoreduction method under UV light irradiation.

The crystal information of the pristine STO and Ag/STO photocatalyst was assessed through XRD analyses, as displayed in Figure 2. The XRD patterns of the samples exhibit typical diffraction peaks of cubic perovskite STO, in which the characteristic peaks at 2θ of 24.807, 26.507, 28.182, 36.620, 43.681, and 47.839 are assigned to (100), (002), (101), (102), (110), and (103) crystal planes respectively (JCPDS no. 74-1296). Furthermore, the peak appearing at $2\theta = 38°$ is produced in STO/Ag nanocubes belonging to the Ag phase about the JCPDS card no. 04-0783. This demonstrated that the AgNPs were deposited successfully on the surface area of STO, which is consistent with the results of the TEM image in Figure 1.

The optical properties of as-prepared specimens are important processes for photo-catalytic reactions. Therefore, the UV−vis spectra were used to investigate the optical characteristic of the photocatalysts (Figure 3). As reflected by Figure 3, the pristine STO photocatalyst shows absorption edges at 388 nm related to a charge transfer from the valence band (VB) to the conduction band (CB), which corresponds to a bandgap energy of 3.2 eV for pristine STO (Figure 3(b)). For the Ag/STO sample case, the Ag/STO photocatalyst exhibits visible-light absorption with an absorption edge at $\sim$ 450 nm due to the LSPR of Ag NPs, which is beneficial for enhancing the photocatalytic HER activity in the visible light.

To evaluate the effect of decorating with Ag on the surface of the $SrTiO_3$ nanocubes for photo-catalytic H_2 evolution activities. The photo-catalytic H_2 evolution performance of photocatalyst was accomplished using water/methanol solution under UV light and visible light, as shown in Figure 4. As observed, the H_2 production of the Ag/$SrTiO_3$ sample exhibited significantly higher than that of the pure STO under experimental conditions. Under UV light, the Ag/STO sample achieved the H_2 evolution of ~ 414 μmol.h^{-1}.g^{-1}, which is ~ 2 times that photocatalyst with the pure STO nanocubes due to efficient charge separation. Interestingly, the amount of H_2 produced by the Ag/STO photocatalyst was ~ 316 μmol.h^{-1}.g^{-1}, roughly 12-times that of the pure STO under visible light, whereas, no appreciable H_2 production was observed under visible light irradiation

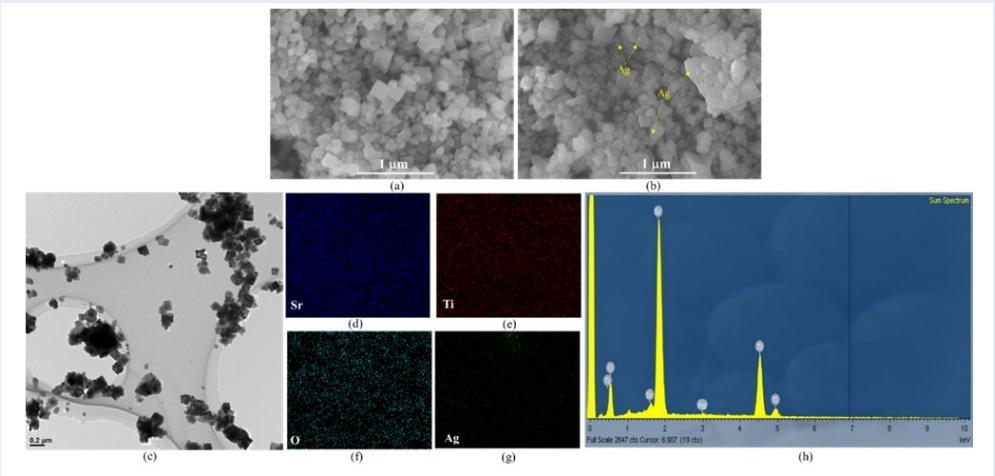

Figure 1: **The morphological features and chemical elements of the pristine STO and the Ag/STO photocatalyst (a, b) SEM image of the pristine STO, and Ag/STO photocatalyst, respectively, (c) TEM image of the Ag/STO specimen, and (d-g) elemental mapping of Sr, Ti, O, and Ag, respectively, (h) EDX spectrum of the Ag/STO heterostructures.**

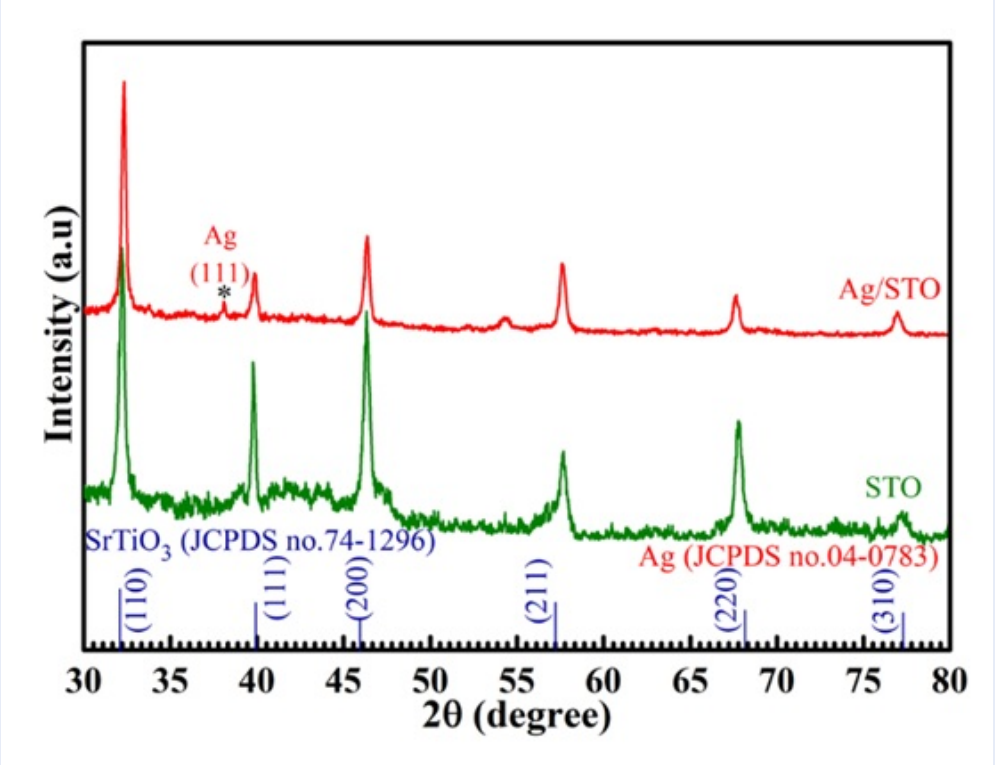

Figure 2: **The crystallinity using XRD patterns of the obtained Ag/STO and pristine STO photocatalyst.**

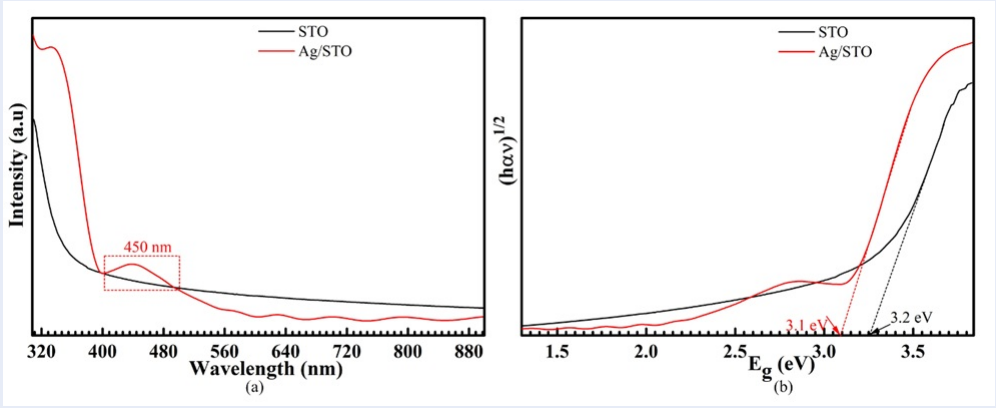

Figure 3: The optical characteristics of the photocatalyst using the UV–Vis diffuse reflectance spectra (a) and plot of (ah)$^{1/2}$ vs. photon energy (b) of the pure STO and the Ag/STO specimen.

of the pure STO nanocubes. This could be attributed to the larger bandgap energy of the single STO that cannot be reached under visible light, leading to low H_2. On the other hand, compared with that of the pure STO, the Ag/STO photocatalyst exhibited outstanding H_2 photo-catalytic activity. Additionally, the reusability of a photocatalyst is also a critical factor for practical applications. The heterostructure of Ag/STO was thus employed for H_2 production under UV light (Figure 5). The H_2 performance of the Ag/STO remained unchanged after 4 cycles, implying that the high durability of the as-obtained photocatalyst.

The photo-catalytic performance of the single STO and Ag/STO photocatalyst was evaluated under photodecomposition of RhB aqueous solution with the existence of UV light and visible light irradiation after 120 min, as shown in Figure 6. It could be clearly observed that no decomposition of the RhB was achieved without the photocatalyst under UV and visible light irradiation, which may be assigned to the low self-degradation of RhB. In contrast, the effective decomposition of RhB in the presence of photocatalyst and light energy source was obtained, thereby indicating that the photocatalyst and light irradiation plays a significant role in the photodegradation activity of RhB solution. Compared with the pure STO, the Ag/STO photocatalyst showed a higher photodegradation of the RhB dye under both UV and visible light exposure. As presented in Figure 6, the Ag/STO photocatalyst exhibited outstanding RhB decomposition with degradation rates of RhB of approximately ~80 % and ~70 % under exposure to UV light and visible light, respectively.

DISCUSSION

The morphological and crystal characteristics of STO did not significantly change after the introduction to Ag nanoparticles by hydrothermal pathway and photo-reduction method as shown in Figure 1 and Figure 2. The photocatalytic degradation of dye molecules and hydrogen evolution reaction (HER) of the Ag/STO photocatalyst was higher than that of the pristine STO under both UV and visible light exposure. This could be explained by i) improvement of absorption ability in the visible light region based on the LSPR effect of AgNP, which efficiently prompted the absorption and separation of the photoinduced electron-hole pairs; ii) the effective separation and transport of the photogenerated charge carriers based on the formation of a Schottky barrier between the Ag and STO, leading to an enhanced photo-catalytic H_2 generation and photodegradation of the RhB dye. Under irradiation with an photon energy equal or greater than the bandgap energy of semiconductor, the photoinduced electron–hole pairs are generated. These photoinduced electrons can reduce organic pollutants or water to form H_2 production. Meanwhile, the photoinduced holes react with dye molecules to generate a strong oxidizing agents, which improve the decomposition of dye molecules into nontoxic products[22]. Based on the above results, to better understand the photo-catalytic improvement of the hybrid photocatalyst compared with the pure photocatalyst, a mechanism of their photo-catalytic activity was discussed. Upon exposure to UV light, STO is excited and generated the photoinduced electron-hole pairs. These electrons jump to the CB and transfer to Ag NPs. They reduce protons (H^+) to generate H_2. Meanwhile, the photogenerated holes on the VB of

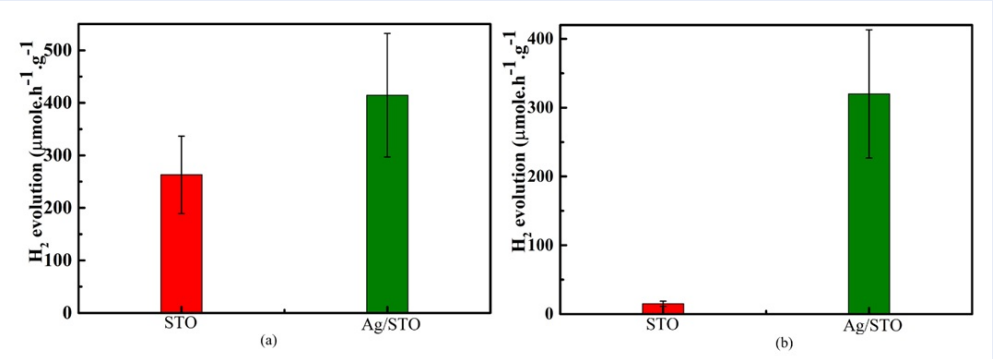

Figure 4: **The photo-catalytic H_2 evolution of the obtained photocatalyst under the different irradiation (a) under UV light, (b) visible light of the STO and Ag/STO photocatalyst.**

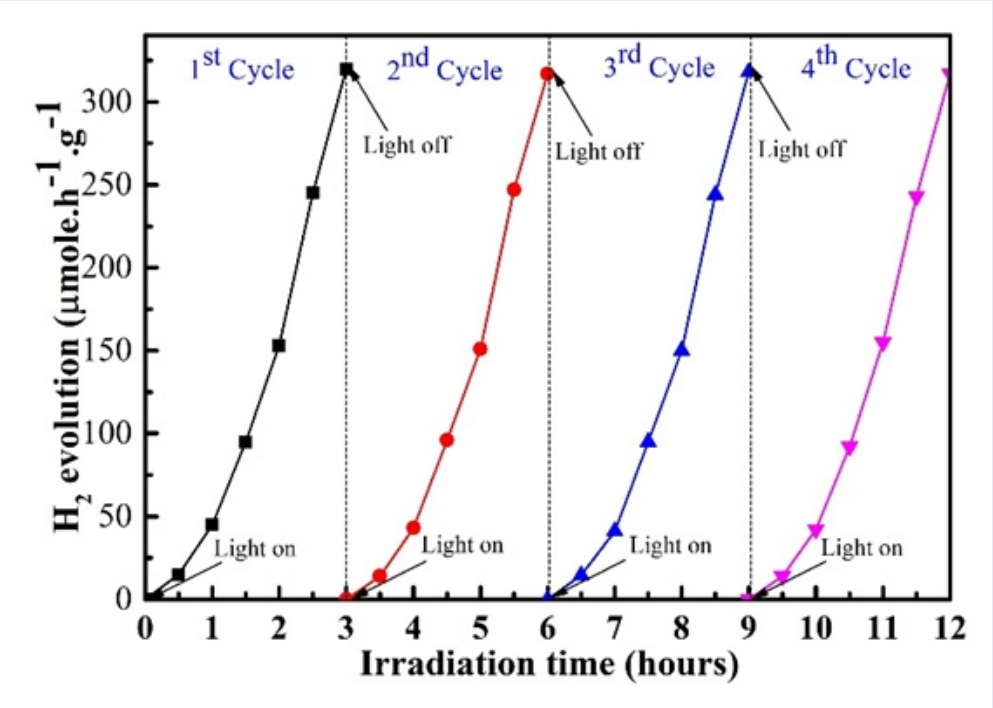

Figure 5: **The recyclability performance for H_2 activity under visible light illumination after 4 cycles of the Ag/STO photocatalyst.**

STO can oxidize the absorbed H_2O molecules into hydroxyl radicals ($OH^{\bullet}$)[23]. Under visible light irradiation, STO cannot be activated because of its large energy gap. Meanwhile, the AgNPs can strongly absorb under the visible light based on the effect of LSPR to form the hot electrons[24]. These hot electrons move to the CB of STO and reduce H^+ to produce H_2 gas. The holes on the Ag surface can react with H_2O to form $OH^{\bullet}$ in a successive reaction route. These formed reactive species decompose RhB molecule dyes into nontoxic products. These outcomes from this work provide new insight into the water-splitting performance and photo-catalytic RhB degradation in practical applications based on the incorporation of perovskite and noble metal.

CONCLUSION

In summary, Ag/STO heterostructures were successfully synthesized by the hydrothermal method and photo-reduction under assisted-UV light. An out-

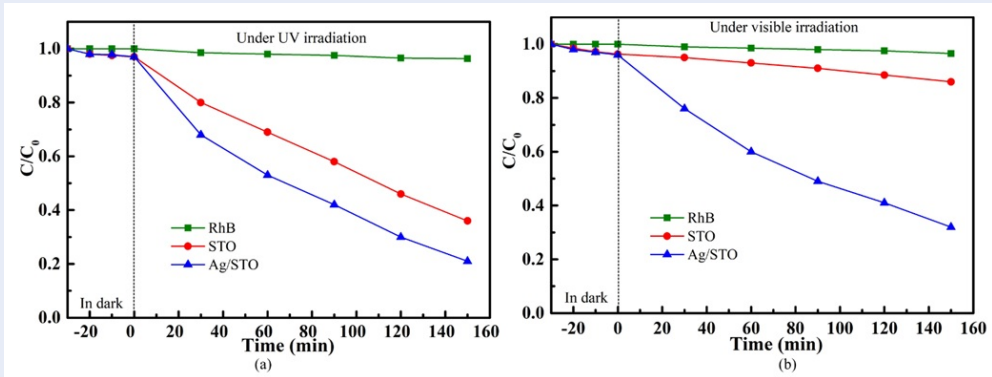

Figure 6: **The photo-catalytic performance of the photocatalyst through decomposition of RhB organic dyes.**

standing photo-catalytic and yield in H_2 evolution reaction of the Ag/STO photocatalyst in comparison with the pristine STO was observed. This could be attributed to the synergetic effect between STO and Ag and the LSPR effect of Ag that was responsible for the effective separation and transportation of the charge carriers and inhibition of the rapid recombination of the photoinduced charge carriers on the Ag/STO hybrid. As a result, the recombination of the photogenerated electron-hole pairs on the photocatalyst was eliminated through the establishment of the Schottky channel, and the strong absorption in the visible light was enhanced via the LSPR effect of AgNPs, providing an efficient charge separation and transfer of the hybrid photocatalyst. Thus, the photo-catalytic activity for the RhB photodegradation efficiency of Ag/STO was ~ 80% and ~ 70% under UV and visible light, respectively. Furthermore, the H_2 evolution rate of the achieved Ag/STO nanocubes was approximately 414 and 316 μmol.h^{-1}.g^{-1} under UV and visible light illumination, respectively. This study can give an efficient pathway for designing the photo-catalytic system for environmental treatment and renewable energy production.

ABBREVIATIONS

Ag: Silver
$SrTiO_3$: Strontium titanate

COMPETING INTERESTS

The authors declare that there is no conflict of interest regarding the publication of this article.

AUTHORS' CONTRIBUTIONS

Ton Nu Quynh Trang has conceived of the present idea, carried out and written the manuscript with support from Vu Thi Hanh Thu. Le Thị Ngoc Tu and Le Lam Anh Phi has supported the analytical techniques.

ACKNOWLEDGEMENTS

Ton Nu Quynh Trang was funded by Vingroup Joint Stock Company and supported by the Domestic Master/PhD Scholarship Programme of Vingroup Innovation Foundation (VINIF), Vingroup Big Data Institute (VINBIGDATA), code [VINIF.2020.TS.08].

REFERENCES

1. Tian J, Zhang Y, Du L, He Y, Jin XH, Pearce S, Eloi JC, Harniman RL, Alibhai D, Ye R, Phillips DL. Tailored self-assembled photo-catalytic nanofibres for visible-light-driven hydrogen production. Nature Chemistry. 2020 Dec;12(12):1150-6;PMID: 33219362. Available from: https://doi.org/10.1038/s41557-020-00580-3.
2. Guo L, Zhong C, Cao J, Hao Y, Lei M, Bi K, Sun Q, Wang ZL. Enhanced photo-catalytic H2 evolution by plasmonic and piezotronic effects based on periodic Al/BaTiO3 heterostructures. Nano Energy. 2019 Aug 1;62:513-20;Available from: https://doi.org/10.1016/j.nanoen.2019.05.067.
3. Fujishima A, Honda K. Electrochemical photolysis of water at a semiconductor electrode. nature. 1972 Jul;238(5358):37-8;PMID: 12635268. Available from: https://doi.org/10.1038/238037a0.
4. Liu Y, Sun Z, Hu YH. Bimetallic co-catalysts for photo-catalytic hydrogen production from water. Chemical Engineering Journal. 2020 Dec 24:128250;Available from: https://doi.org/10.1016/j.cej.2020.128250.
5. Zhang X, Peng T, Song S. Recent advances in dye-sensitized semiconductor systems for photo-catalytic hydrogen production. Journal of Materials Chemistry A. 2016;4(7):2365-402;Available from: https://doi.org/10.1039/C5TA08939E.
6. Trang TN, Nam ND, Ngoc Tu LT, Quoc HP, Van Man T, Ho VT, Thu VT. In Situ Spatial Charge Separation of an Ir@TiO2 Multiphase Photosystem toward Highly Efficient Photocatalytic Performance of Hydrogen Production. The Journal of Physical Chemistry C. 2020 Jul 10;124(31):16961-74;Available from: https://doi.org/10.1021/acs.jpcc.0c03590.
7. Li X, Zhao H, Liang J, Luo Y, Chen G, Shi X, Lu S, Gao S, Hu J, Liu Q, Sun X. A-site perovskite oxides: an emerging functional material for electrocatalysis and photocatalysis. Journal of Materials Chemistry A. 2021;9(11):6650-70;Available from: https://doi.org/10.1039/D0TA09756J.

8. Yin WJ, Weng B, Ge J, Sun Q, Li Z, Yan Y. Oxide perovskites, double perovskites and derivatives for electrocatalysis, photocatalysis, and photovoltaics. Energy & Environmental Science. 2019;12(2):442-62;Available from: https://doi.org/10.1039/C8EE01574K.
9. Zulueta YA, Lim TC, Dawson JA. Defect clustering in rare-earth-doped BaTiO3 and SrTiO3 and its influence on dopant incorporation. The Journal of Physical Chemistry C. 2017 Oct 26;121(42):23642-8;Available from: https://doi.org/10.1021/acs.jpcc.7b08500.
10. Ma X, Cui X, Zhao Z, Melo MA, Roberts EJ, Osterloh FE. Use of surface photovoltage spectroscopy to probe energy levels and charge carrier dynamics in transition metal (Ni, Cu, Fe, Mn, Rh) doped SrTiO3 photocatalysts for H2 evolution from water. Journal of Materials Chemistry A. 2018;6(14):5774-81;Available from: https://doi.org/10.1039/C7TA10934B.
11. Mu L, Zhao Y, Li A, Wang S, Wang Z, Yang J, Wang Y, Liu T, Chen R, Zhu J, Fan F. Enhancing charge separation on high symmetry SrTiO3 exposed with anisotropic facets for photo-catalytic water splitting. Energy & Environmental Science. 2016;9(7):2463-9;Available from: https://doi.org/10.1039/C6EE00526H.
12. Qureshi M, Garcia-Esparza AT, Jeantelot G, Ould-Chikh S, Aguilar-Tapia A, Hazemann JL, Basset JM, Loffreda D, Le Bahers T, Takanabe K. Catalytic consequences of ultrafine Pt clusters supported on SrTiO3 for photo-catalytic overall water splitting. Journal of Catalysis. 2019 Aug 1;376:180-90;Available from: https://doi.org/10.1016/j.jcat.2019.06.045.
13. Chen BR, Crosby LA, George C, Kennedy RM, Schweitzer NM, Wen J, Van Duyne RP, Stair PC, Poeppelmeier KR, Marks LD, Bedzyk MJ. Morphology and CO Oxidation Activity of Pd Nanoparticles on SrTiO3 Nanopolyhedra. ACS Catalysis. 2018 Apr 16;8(6):4751-60;Available from: https://doi.org/10.1021/acscatal.7b04173.
14. Qureshi M, Garcia-Esparza AT, Jeantelot G, Ould-Chikh S, Aguilar-Tapia A, Hazemann JL, Basset JM, Loffreda D, Le Bahers T, Takanabe K. Catalytic consequences of ultrafine Pt clusters supported on SrTiO3 for photo-catalytic overall water splitting. Journal of Catalysis. 2019 Aug 1;376:180-90;Available from: https://doi.org/10.1016/j.jcat.2019.06.045.
15. Zhao Z, Willard EJ, Li H, Wu Z, Castro RH, Osterloh FE. Aluminum enhances photochemical charge separation in strontium titanate nanocrystal photocatalysts for overall water splitting. Journal of Materials Chemistry A. 2018;6(33):16170-6;Available from: https://doi.org/10.1039/C8TA05885G.
16. Atkinson I, Parvulescu V, Cusu JP, Anghel EM, Voicescu M, Culita D, Somacescu S, Munteanu C, Šćepanović M, Popovic ZV, Fruth V. Influence of preparation method and nitrogen (N) doping on properties and photo-catalytic activity of mesoporous SrTiO3. Journal of Photochemistry and Photobiology A: Chemistry. 2019 Jan 1;368:41-51;Available from: https://doi.org/10.1016/j.jphotochem.2018.09.019.
17. Tao R, Li X, Li X, Shao C, Liu Y. TiO2/SrTiO3/gC3N4 ternary heterojunction nanofibers: gradient energy band, cascade charge transfer, enhanced photo-catalytic hydrogen evolution, and nitrogen fixation. Nanoscale. 2020;12(15):8320-9;PMID: 32236215. Available from: https://doi.org/10.1039/D0NR00219D.
18. Ahmadi M, Dorraji MS, Rasoulifard MH, Amani-Ghadim AR. The effective role of reduced-graphene oxide in visible light photo-catalytic activity of wide band gap SrTiO3 semiconductor. Separation and Purification Technology. 2019 Dec 1;228:115771;Available from: https://doi.org/10.1016/j.seppur.2019.115771.
19. Yan Y, Yang H, Yi Z, Li R, Wang X. Enhanced photo-catalytic performance and mechanism of Au@CaTiO3 composites with Au nanoparticles assembled on CaTiO3 nanocuboids. Micromachines. 2019 Apr;10(4):254;PMID: 30999566. Available from: https://doi.org/10.3390/mi10040254.
20. Guo L, Zhong C, Cao J, Hao Y, Lei M, Bi K, Sun Q, Wang ZL. Enhanced photo-catalytic H2 evolution by plasmonic and piezotronic effects based on periodic Al/BaTiO3 heterostructures. Nano Energy. 2019 Aug 1;62:513-20;Available from: https://doi.org/10.1016/j.nanoen.2019.05.067.
21. Xu S, Guo L, Sun Q, Wang ZL. Piezotronic effect enhanced plasmonic photocatalysis by AuNPs/BaTiO3 heterostructures. Advanced Functional Materials. 2019 Mar;29(13):1808737;Available from: https://doi.org/10.1002/adfm.201808737.
22. Girija K, Thirumalairajan S, Mastelaro VR, Mangalaraj D. Photocatalytic degradation of organic pollutants by shape selective synthesis of β-Ga2O3 microspheres constituted by nanospheres for environmental remediation. Journal of Materials Chemistry A. 2015;3(6):2617-27;Available from: https://doi.org/10.1039/C4TA05295A.
23. Habibi-Yangjeh A, Akhundi A. Novel ternary g-C3N4/Fe3O4/Ag2CrO4 nanocomposites: magnetically separable and visible-light-driven photocatalysts for degradation of water pollutants. Journal of Molecular Catalysis A: Chemical. 2016 May 1;415:122-30;Available from: https://doi.org/10.1016/j.molcata.2016.01.032.
24. Shang M, Hou H, Gao F, Wang L, Yang W. Mesoporous Ag@TiO2 nanofibers and their photocatalytic activity for hydrogen evolution. RSC advances. 2017;7(48):30051-9;Available from: https://doi.org/10.1039/C7RA03177G.